UNCLASSIFIED CONFIDENTIAL

Copy 6
RM E54F24

3 1176 00121 0237

NACA RM E54F24

NACA

RESEARCH MEMORANDUM

EXPERIMENTAL INVESTIGATION OF A FIVE-STAGE AXIAL-FLOW RESEARCH COMPRESSOR WITH TRANSONIC ROTORS IN ALL STAGES

I - COMPRESSOR DESIGN

By Donald M. Sandercock, Karl Kovach, and Seymour Lieblein

Lewis Flight Propulsion Laboratory
Cleveland, Ohio

CLASSIFICATION CHANGED
UNCLASSIFIED

To

By authority of Navy PA 3 effective Date 12-3-58
NB 2-13-59

LIBRARY COPY
SEP 1954
LANGLEY AERONAUTICAL LABORATORY
LIBRARY, NACA
LANGLEY FIELD, VIRGINIA

CLASSIFIED DOCUMENT

This material contains information affecting the National Defense of the United States within the meaning of the espionage laws, Title 18, U.S.C., Secs. 793 and 794, the transmission or revelation of which in any manner to an unauthorized person is prohibited by law.

NATIONAL ADVISORY COMMITTEE
FOR AERONAUTICS

WASHINGTON

September 8, 1954

CONFIDENTIAL

UNCLASSIFIED

NATIONAL ADVISORY COMMITTEE FOR AERONAUTICS

RESEARCH MEMORANDUM

EXPERIMENTAL INVESTIGATION OF A FIVE-STAGE AXIAL-FLOW RESEARCH COMPRESSOR WITH TRANSONIC ROTORS IN ALL STAGES

I - COMPRESSOR DESIGN

By Donald M. Sandercock, Karl Kovach, and Seymour Lieblein

3198

CT-1

SUMMARY

A five-stage axial-flow compressor with all rotor rows operating with transonic relative inlet Mach numbers was designed as a research unit to study the potentialities and problems arising from the compounding of transonic stages. The compressor was designed as a component of an existing turbojet engine.

At a tip speed of 1100 feet per second, the compressor was designed to produce an over-all total-pressure ratio of 5 at a corrected specific weight flow of 31 pounds per second per square foot of rotor frontal area. With the absolute velocities axial at the inlet to all rotor rows, rotor tip relative Mach numbers varied from 1.18 in the first stage to 0.90 in the fifth stage. Constant total enthalpy and constant entropy from hub to tip were used in the velocity-diagram construction. Stage total-pressure ratios were determined from considerations of allowable blade loading as expressed in terms of the blade-element diffusion factor.

This report presents all design values and procedures, blade-row velocity diagrams, and the selection of blade shapes.

INTRODUCTION

The requirements of effective aircraft propulsion indicate the desirability of operating lightweight compact turbojet engines that are highly efficient over wide ranges. For turbojet engines incorporating the multistage axial-flow compressor, reduction in compressor size and weight can be effected by increasing stage pressure ratio (reducing the number of stages required to produce the desired pressure ratio) and increasing mass flow per unit frontal area. These requirements for higher levels of stage performance can theoretically be met by increasing

the inlet Mach number relative to the rotor. An indication of the potential gains in these performance characteristics as the maximum inlet rotor Mach number is increased from 0.75 to 1.10 is given in reference 1.

It is demonstrated in references 2 and 3 that axial-flow compressor rotors and stages of high pressure ratio (1.35 to 1.50), and high specific mass flow (28 to 34 lb/(sec)(sq ft of frontal area)), while maintaining high efficiency (approx. 0.90), can be obtained by designing for operation in the transonic region of rotor relative inlet Mach numbers. Stator-outlet conditions and general performance of the transonic inlet stage appear satisfactory for purposes of multistaging with succeeding stages of conventional design (ref. 2). Reference 4 illustrates the favorable results that have been obtained by employing transonic rotors in the first two stages of a multistage compressor.

3198

It is also speculated that transonic rotor operation need not be restricted to inlet stages. Further increases in average stage pressure ratio might be realized if all of the rotors of a multistage machine were designed to operate at higher than conventional levels of relative inlet Mach number. A further reduction in the total number of stages might then be obtained. However, several important observations can be made about all-transonic operation. In order to maintain high relative inlet Mach numbers in succeeding rotor rows and still obtain a low compressor-discharge velocity, it is necessary, with high-pressure-ratio rotors, to employ stator turning angles of greater magnitude (up to about 45°) than those occurring in conventional designs. A recent investigation of high-turning axial-discharge stator blades (ref. 5), however, indicates that practically no sacrifice in stage design-point efficiency need result with the use of highly cambered stators if moderate stator blade loadings (as discussed in ref. 6) and best incidence angles are obtained. Secondly, while the single-stage transonic compressors exhibited good performance in the off-design regions of operation, certain characteristics indicate the possibility of off-design problems in a multistage unit. Because of the reduced range of operation (loss against incidence-angle characteristics) of rotor blade sections at high inlet Mach numbers (ref. 1), the compromises in blade setting that may be desirable to aid part-speed performance may be limited for both the outlet and inlet stages.

In view of these considerations, an experimental five-stage axial-flow compressor was designed and constructed at the NACA Lewis laboratory to investigate the potentials and problems of a high-stage-pressure-ratio compressor obtained by the use of transonic rotors in all stages. The compressor was designed for an average stage pressure ratio of 1.38 with stators operating at conventional inlet Mach numbers but turning the flow back to the axial direction. The compressor was installed and operated as a component of an existing turbojet engine. This report summarizes the design procedure and includes the calculation of the velocity

diagrams and the selection and design of blade shapes. The over-all performance of the compressor over the operating range of 40 to 100 percent of equivalent design speed is presented in reference 7.

SYMBOLS

The following symbols are used in this report:

A_f	compressor frontal area, 2.18 sq ft
a	velocity of sound, ft/sec
c	blade chord length, in.
D	diffusion factor (ref. 6)
g	acceleration due to gravity, 32.17 ft/sec^2
H	total enthalpy, sq ft/sec^2
i	incidence angle, angle between inlet relative air-velocity vector and tangent to blade mean line at leading edge, deg
K	wall boundary-layer blockage factor
M	absolute Mach number
M'	relative Mach number
P	absolute total pressure, lb/sq ft
p	static pressure, lb/sq ft
R	gas constant for air, ft/$^\circ$R, 53.35
r	radius measured from axis of rotation, ft
s	entropy, sq ft/(sec^2)($^\circ$R)
T	absolute total temperature, $^\circ$R
t	static temperature, $^\circ$R
U	blade speed, ft/sec
V	absolute velocity of air, ft/sec

3198 CT-1 back

V' velocity of air relative to blade row, ft/sec

W weight flow of air, lb/sec

x distance along axis, ft

z ratio of radius to tip radius

β absolute air-flow angle measured from axial direction, deg

β' air-flow angle relative to blade row measured from axial direction, deg

$\Delta\beta'$ air turning angle, change in relative flow angle from inlet to outlet of blade row, deg

β^* air-flow angle measured on streamline (tangent) plane (see fig. 4), deg

γ ratio of specific heats for air, 1.40

γ° blade angle, angle between tangent to blade mean line at leading or trailing edge and axial direction, deg

δ° deviation angle, angle between outlet relative air-velocity vector and tangent to blade mean line at trailing edge, deg

ε angle of streamline plane across blade row, computed from radius change and axial depth across blade row, deg

η adiabatic temperature-rise efficiency

θ distance in tangential direction

ξ chord angle, angle between blade chord line and axial direction, deg

ρ static density of air, lb/cu ft

σ solidity, ratio of blade chord to blade spacing

φ camber angle, difference between blade angles at inlet and outlet of blade row, deg

Subscripts:

f.s. free stream

h hub

3198

[redacted]

id	ideal
m	mean
n	axial station location number (from 0 to 13, fig. 2)
R	rotor
r	radial direction
T	total or stagnation conditions
t	tip
x	axial direction
θ	tangential direction

Numbered subscripts refer to axial stations

3198

OVER-ALL DESIGN

The research compressor was designed for installation in an existing turbojet engine in order to obtain a convenient power source. Accordingly, geometry and over-all design specifications of the compressor are governed to a large extent by the mechanical and aerodynamic characteristics of the test engine and its components. The following over-all characteristics were chosen for the design of the five-stage transonic research compressor:

(1) Total-pressure ratio = 5.0 (average stage total-pressure ratio = 1.38)

(2) Compressor rotor outer diameter, 20 in. (constant)

(3) Inlet hub-tip radius ratio, 0.50

(4) Tip speed, 1100 ft/sec

(5) Inlet axial Mach number, 0.6 (inlet axial velocity = 648 ft/sec at standard inlet conditions)

(6) Discharge axial velocity, 520 ft/sec

(7) Constant radial work input

[redacted]

For an assumed value of wall boundary-layer blockage at the compressor inlet of 1 percent, these design values give a corrected weight flow of 67.5 pounds per second, corresponding to a specific weight flow of 31 pounds per second per square foot of rotor frontal area. Because of the approximate symmetry of casing fairing at the first rotor inlet (station 2), the axial velocity at the inlet to the first rotor row was considered to be constant across the radial height of the annulus. The 1100-foot-per-second tip speed and 0.60 inlet axial Mach number combine to give a relative Mach number of 1.18 at the tip of the first rotor row.

3198

The magnitude of the compressor-outlet axial velocity was determined after consideration of the existing diffuser and combustor designs. In general, since desired combustor-inlet velocity is much lower than the compressor-inlet velocity, the question arises as how to distribute the diffusion in axial velocity between compressor and diffuser. Large amounts of axial-velocity diffusion in the compressor will tend to reduce the pressure ratio corresponding to a given value of design blade loading (diffusion factor of ref. 6), while large amounts of diffusion after the compressor might require diffuser sections of excessive length. The outlet axial velocity chosen was believed compatible with the diffuser capability and compressor blade loading.

STAGE DESIGN

The number of stages required to produce the desired over-all pressure ratio of 5 was determined from preliminary calculations of average stage pressure ratios obtainable from reasonable values of blade loading at the design tip speed of the compressor.

Adiabatic Efficiency

The prediction of the adiabatic efficiency of an axial-flow compressor presents a very complex problem, since a detailed knowledge of the flow losses is involved. Consequently, efficiencies are generally assumed, based on previous experience. From considerations of references 1 and 5, the adiabatic efficiency of the first stage was assumed to be 0.89. Over stages 2 to 5 a continual decrease in stage efficiency was assumed, since the hub and casing boundary layers influence an increasing portion of the blade span as the flow area is decreased across the compressor. Stage efficiencies selected are given in table I. For the design compressor total-pressure ratio of 5, these stage efficiencies give an over-all efficiency of approximately 0.85.

3198

Axial Velocity

In order that transonic-rotor relative inlet Mach numbers be maintained in succeeding stages, and for simplicity in the design calculations, axial discharge (no outlet rotation) from each stator row was prescribed. This design condition, combined with the velocity-diagram assumptions of constant enthalpy, constant entropy, and equilibrium of static pressure from hub to tip, results in an axial velocity that is radially constant at all stations (see appendix A). The prescribed diffusion of the axial velocity across the compressor was approximately uniformly distributed among the stages (table I).

Pressure Ratio

The stagewise distribution of total-pressure ratio was chosen from considerations of individual stage blade-loading limitation and of off-design performance characteristics. According to reference 8, improved off-design performance is obtained by lightly loading the inlet stage, designing the intermediate stages close to their loading limit, and moderately loading the exit stages. For this design, a measure of the blade loading was obtained by means of the diffusion factor of reference 6. For both rotor and stator, the diffusion factor, which indicates blade loading by serving as a measure of the blade suction-surface velocity gradient, is defined in terms of the blade-row velocity diagrams by

$$D = \left(1 - \frac{V'_n}{V'_{n-1}}\right) + \frac{V'_{\theta,n-1} - V'_{\theta,n}}{2\sigma V'_{n-1}} \qquad (1)$$

From the terms of equation (1) and consideration of velocity-triangle relationships, it is apparent that the diffusion factor is a function of the change of tangential velocity across a blade row (measure of the blade-row pressure ratio), solidity, axial-velocity ratio, and air inlet angle.

Experience has shown that, for a typical transonic stage, the value of design diffusion factor in the rotor tip region is a critical determinant of the efficiency of the stage (ref. 1). Accordingly, a stagewise distribution of total pressure at the tip section was obtained to correspond with the suggested stagewise variation of blade loading (diffusion factor). The procedure used was to assume several values of rotor pressure ratio and from the prescribed values of rotor efficiency, axial velocity across the rotor, and solidity, to compute the rotor blade tip diffusion factors. Final values of stage pressure ratio were chosen to give a reasonable variation of diffusion factor as indicated by the loss correlations of reference 6 and to match the desired over-all pressure ratio.

The stepwise procedure used for determining the stage design characteristics was as follows:

(1) Average axial velocity at the outlet of each stage is known from the prescribed distribution of axial velocity across the compressor. On the basis of experience, all the drop in stage average axial velocity was assumed to occur across the rotor. For the type of design used herein, in which the axial velocity is constant radially, the average value of axial velocity is identical to the local value at the tip for rotor and stator.

3198

(2) Rotor blade tip solidities were selected according to previous transonic experience.

(3) Several values of stage total-pressure ratio were assumed and stage total-temperature ratio computed from the prescribed value of stage efficiency (table I) and equation (A7). Assuming no change in total temperature across the stator row and a rotor efficiency 2 points higher than the stage efficiency, rotor total-pressure ratio was computed.

(4) From equation (A6) and the rotor pressure ratio values of step (3), the change in tangential velocity across the rotor was determined.

(5) From the rotor-inlet and -outlet velocity-diagram components (steps (1) and (4)) and the selected values of rotor tip solidity (step (2)), rotor tip diffusion factors were computed from equation (1).

(6) A stage total-pressure ratio was chosen to give a reasonable value of rotor tip diffusion factor as selected from considerations of the suggested stagewise variations of blade loading.

(7) The procedure outlined in steps (1) to (6) was then applied to each succeeding stage across the compressor.

(8) Stage total-pressure ratios and rotor blade tip solidities were adjusted slightly to obtain both the desired over-all total pressure ratio and distribution of diffusion factor.

The efficiencies given in table I and used in this procedure were representative of mass-averaged efficiencies that include the losses in the wall boundary layers. Strictly speaking, since these and subsequent velocity-diagram calculations are intended to represent the free-stream portions of the flow (central region of blade height where efficiencies are comparatively high), average blade-element efficiencies which consider only the losses associated with the flow around the blade element should be employed. According to reference 9, it would be desirable, furthermore, to consider the effects on the design velocity distributions due to any radial variations of entropy (blade-element efficiency) that

may exist in the free-stream region. This procedure may be especially desirable in the later stages. A similar consideration applies to the values of total-pressure ratio used in the velocity-diagram calculations. In this more specific calculation procedure, which essentially represents the free-stream flow distributions, the defects in total-pressure ratio and efficiency in the wall boundary-layer regions at hub and tip would have to be estimated in some manner in order to obtain a measure of the compressor mass-averaged total-pressure ratio and efficiency.

3198

Boundary-Layer Blockage Factor

CL-2

As indicated in the previous section, at any axial station between blade rows, the design approach considered that the flow across the annulus was divided into two distinct portions, a main or free-stream portion where the viscosity effects of the fluid on the flow are small, and a small portion near the casing walls known as the wall boundary layer where the viscosity effects on the flow become appreciable. A typical radial variation of the product ρV_x might then appear as shown by the solid line in figure 1. Integrated weight flow at the axial station is given by

$$W = 2\pi \int_{r_h}^{r_t} (\rho V_x) r \, dr \tag{2}$$

where (ρV_x) refers to local values along the radius.

Since the design equations used herein consider only the free-stream flow, and since it was convenient to work with the geometric limits of hub and tip radius, an ideal weight flow, or weight flow computed as if no wall boundary layers existed, was defined by

$$W_{id} = 2\pi \int_{r_h}^{r_t} (\rho V_x)_{f.s.} \, r \, dr \tag{3}$$

where the $(\rho V_x)_{f.s.}$ are the free-stream values extrapolated to the wall boundaries (dotted line in fig. 1). The actual weight flow may then be related to the ideal weight flow by means of the blockage factor K, as

$$W = KW_{id}$$

or

$$W = 2\pi K \int_{r_h}^{r_t} (\rho V_x)_{f.s.} \, r \, dr \tag{4}$$

[redacted]

The boundary-layer blockage factor then serves as a measure of the wall boundary-layer displacement thickness. It should be noted that the blockage factor as defined bears no relation to the free-stream efficiencies, since only blade-element losses should be considered in the computation of density and axial velocity in equation (4). The blockage factor, as a displacement thickness, however, will be proportional to the loss in total pressure and efficiency in the wall boundary-layer regions and will, therefore, be a measure of the relation between average free-stream (velocity-diagram) conditions and mass-averaged conditions.

A value of K of 0.95 at the outlet of the first stage was obtained from previous transonic-compressor experience (ref. 5), and an approximately linear variation to 0.90 at the compressor discharge was assumed. The stagewise distribution of K is shown in table I.

Although the concept of a division of the flow into viscous and nonviscous regions is indicated by experience to be an adequate representation of the flow in the inlet stages, it is recognized that such a division may not be representative of the flow in the later stages, where, because of the comparatively short blade heights, the viscous effects extend over a much greater portion of the passage height, and the ρV_x product will tend to approach a more parabolic form (as in pipe flow). In such cases, a strict division of the flow into free-stream and boundary-layer regions might be difficult. For the five-stage design, however, for simplicity, the blockage-factor concept was used in all stages.

Hub Contour

With stage total-pressure ratio, total-temperature ratio, boundary-layer blockage factor K, and average stator-outlet axial velocity V_x known, the annulus area, and therefore the hub radius ratio, at the outlet of each stage was computed from equation (B6).

With hub radius ratio values computed at each stage exit, axial chord lengths and axial clearances between blade rows were selected and a smooth hub profile drawn through these points. Because this compressor was designed as a research compressor, axial spacings of 3/4 inch behind each rotor row and $1\frac{1}{8}$ inches behind each stator row were maintained to permit the use of survey instruments.

In view of the large axial blade-row clearances and the low blade aspect ratios (blade chord lengths are discussed in a later section), as indicated in reference 10, the effects of streamline curvature in the radial-axial plane on the radial equilibrium of the flow were considered negligible. However, in view of the sensitivity of transonic-rotor

[redacted]

performance to incidence angle, the change in axial velocity across the relatively large axial clearance between stator trailing edge and rotor leading edge was taken into account by the adoption of two computational stations between the stator and rotor. The stator-outlet stations, where stage design characteristics were prescribed, are designated by even numerals, and the rotor inlets by lettered stations. A sketch of the passage contour of the compressor showing the various blade-row-inlet and -outlet stations is presented in figure 2.

3198

Velocity Diagram

Velocity diagrams were computed at the inlet and outlet of each blade row for six equally spaced positions along the blade height. For simplicity, the streamlines across a blade row were assumed to lie along conic surfaces. A sketch illustrating the assumed and true streamlines is shown in figure 3, and the velocity and angle relations in the tangent plane are shown in figure 4. In determining the flow streamline path, since the type of design which gives a radially constant axial velocity shows very small mass-flow shifts across a blade row, the radial passage height at each computational plane was divided into the same number of equal radial increments and the streamlines were assumed to pass through these points. Thus, for a given streamline, at each axial station,

$$\frac{r_t - r}{r_t - r_h} = \text{constant} \tag{5}$$

where r is the radius at which the streamline intersects the computational plane. For computational purposes, a general expression involving radius ratio $z = r/r_t$ was written to give the radius ratio z_n of a particular streamline at any axial station n for a given radius ratio z_2 at inlet station 2 as

$$z_n = 1 - (1 - z_2)\frac{1 - z_{h,n}}{1 - z_{h,2}} \tag{6}$$

Values of the radius ratio along the hub streamline were obtained from the layout of the hub contour.

The various conditions and assumptions and the complete equations used in the calculation of stage velocity diagrams in the streamline (tangent) plane are presented in appendix A. In the numerical calculations for this design, the radial angle terms in the velocity-diagram calculations were neglected, because the largest value of tangent-plane angle ε was relatively small (maximum value about 12° at the hub of the first rotor). The step-by-step procedure used to calculate the velocity diagrams was as follows:

(1) Total temperature at the inlet to a stage was computed from the data of table I and equation (A7).

(2) Rotor-inlet relative velocities and angles were computed from equations (A12) and (A13). For the second to fifth rotors, the axial velocity at the rotor inlet (lettered stations) was determined from the axial velocity at the stator outlet of the preceding stage and from considerations of the change in annulus area between the two station locations.

(3) Absolute tangential velocities at the rotor outlet were computed from equations (A6) as described in the pressure ratio section and (A3).

(4) Axial velocity at rotor outlet was obtained from a trial-and-error solution of the continuity integral (eq. (A8)). Several values of axial velocity were selected and corresponding values of density and weight flow were computed from equations (A9), (A10), and (A8). The correct value of axial velocity was then obtained from the graphical intersection of computed and design weight flows.

(5) Velocity diagrams at rotor outlet (stator inlet) were computed from equations (A14) to (A17).

(6) The magnitude and direction of the stator-outlet velocities were given by the design requirement of axial discharge of the flow from the stator row and the prescribed values of stage-outlet axial velocity (table I).

A schematic sketch of a typical stage velocity diagram at hub and tip is shown in figure 5, and tabulated values of velocity and angle in the tangent plane at the six radial design positions are listed for all stages in tables II (rotor velocity diagrams) and III (stator velocity diagrams).

BLADE DESIGN

Rotor

The blade shape selected for the rotor was the double-circular-arc profile consisting of circular-arc pressure and suction surfaces. Experiences with transonic rotors at the time indicated that the double circular arc was a satisfactory blade shape for transonic operation (see refs. 11 and 12 for considerations of transonic blade shapes). The circular-arc blade has the added advantage of simplicity of design and analysis.

3198

3198

The large reduction of low-loss range of incidence angle as Mach number is increased (ref. 5) makes the selection of incidence angle an important consideration in transonic multistage design. From considerations of limited available high Mach number data (refs. 5 and 13), a constant positive incidence angle of 4° was selected for all radii and all rotor blade rows.

Camber angle. - Figure 6 shows the geometric relations between incidence angle, turning angle, and deviation angle necessary to compute the blade camber angle, which is given by

$$\varphi = \Delta\beta' + \delta^\circ - i \tag{7}$$

For fixed values of incidence angle, the camber angle required for the design air turning angle is then determined from the deviation-angle characteristics of the blade shape. Deviation angle (fig. 6) is the difference between the direction of the outlet air and the tangent to the blade mean line at the trailing edge.

At the time of design, no deviation-angle rules were known that had proven accurate for this type of design. For the first two stages, in view of the similarity between this design and the design and performance of the transonic rotor of reference 2, the design values of deviation angle were selected to correspond to the deviation angles of the rotor of reference 2. For the other stages, which were designed at a somewhat later date, it was found that, for a fixed incidence angle of 4°, the deviation angle can be approximated by the empirical relation

$$\delta^\circ = \frac{0.405\varphi}{\sigma - \frac{1}{2}\sin\xi} \tag{8}$$

obtained from a survey of a limited amount of circular-arc transonic-rotor data. In the calculation of camber and deviation angles as given by equations (7) and (8), an iteration was required for assumed values of camber necessary for the evaluation of the chord angle ξ. Design values of deviation and camber angle are given in table IV. More recent considerations of deviation-angle characteristics for circular-arc blades are given in references 1 and 13.

Blade construction. - A compressor blade is designed as a radial stacking of a number of individual blade elements. For ease of manufacture, it was desirable that the coordinates of a blade element be specified on a plane perpendicular to the radial stacking line of the blade (hereafter called the horizontal plane). Since all computed air and blade properties lie along the streamline (tangent) plane, it was necessary to obtain these blade properties on a horizontal plane. Computed

blade angles at the blade inlet and outlet were projected to the horizontal plane by means of geometric considerations that incorporated corrections necessary because the blade leading and trailing edges were not radial elements. The projected blade angles were then plotted against the respective radius. From these plots, inlet and outlet blade angles for a given radius were obtained and a blade camber angle in the horizontal plane for that radius was computed from the difference between the blade angles at the inlet and outlet.

3198

To further simplify the calculation of blade coordinates and the fabrication of the blades, the desired circular-arc mean line was assumed along the horizontal blade element. Around this circular-arc mean line was wrapped a thickness as defined by circular-arc pressure and suction surfaces that pass through the maximum thickness point at the 50-percent chord station and are tangent to 0.015-inch-radius circles with centers at the end points of the mean line.

Although the blade sections on the streamline plane do not have the desired circular-arc mean line in the inlet stages, little difficulty is anticipated in obtaining the design flow conditions in the hub region, inasmuch as calculations in reference 1 indicate that small errors in relative air outlet angle at the hub of this type of transonic inlet stage will have a relatively small effect on rotor performance. The correct establishment of blade profiles in the streamline plane should be particularly desirable for designs in which the tip diameter is varied across the blade row, in view of the increased sensitivity of the tip-region flow to angle errors (ref. 1).

Radial variations of maximum thickness were selected from both aerodynamic and stress considerations. To decrease the blade stress due to the centrifugal forces, a hyperbolic radial variation of maximum thickness with thin tip sections has been found desirable. The thin tip sections are also desirable aerodynamically for the high inlet Mach numbers encountered in the tip region. Maximum blade thickness at the hub was chosen so that, on the basis of one-dimensional area considerations, the blade sections at the hub showed no choking difficulties.

Blade-element properties on the horizontal plane are presented in table IV. For stages 4 and 5, since the angle that the streamline plane makes with the horizontal is very small (maximum of 4° at hub of fourth rotor row), the blade properties on the horizontal plane were assumed to be the same as those calculated for the streamline plane.

Blade chord lengths were selected on the basis of previous transonic experience (ref. 2) and structural considerations involving blade strength, shaft critical speed, and existing engine construction. Axial and actual chord lengths are presented in table IV. Recent unpublished data (also refs. 3 and 14) indicate that efficient transonic-rotor operation can be obtained with blades having shorter chord lengths. Rotor blades were constructed of a heat-treated alloy steel.

[redacted]

3198

Stator

In the first two stator rows, the double-circular-arc blade (circular-arc pressure and suction surfaces) was used (as in refs. 2 and 5), and for the last three stages, where the inlet Mach numbers were reduced, a 65-series thickness distribution of reference 15 was modified and used in conjunction with the circular-arc mean line. The 65-series thickness distribution was used from the leading edge to the 60-percent-chord point, but from there the conventional thickness distribution was modified by using a linear fairing from the 60-percent-chord point to an 0.8-percent-chord radius at the trailing edge. The coordinates of the modified 65-series thickness distribution (i.e., normal to the mean line) for a 10-percent maximum thickness are shown in table VI. Coordinates for other values of maximum thickness were scaled proportionately. The first two rows of double-circular-arc stator blades were set at an incidence angle of 0°; while, because of the increased camber angles, the last three rows of 65-series type stator blades were set at an incidence angle of -2°.

Camber angles were determined from a deviation-angle rule very similar to equation (8), except that a radially varying value of the constant in the numerator of equation (8) was found desirable from a correlation of limited available stator data. The radial variation of the constant used in equation (8) is presented in figure 7 for values of radius ratio because of the large variation of blade span over which the equation was applied. Again, more recent considerations of deviation-angle characteristics are given in reference 1. As was done for the rotor blades, a hyperbolic spanwise distribution of maximum thickness was employed. Design values of the pertinent parameters of the stators are given in table III in the streamline planes and in table V in the horizontal planes. Because the angle between the streamline and the axial direction for stator rows of stages 3 to 5 was small (less than 5° for any blade element), the blade properties calculated along streamline planes were assumed to exist along the horizontal planes for these stages. The first two stator rows were machined alloy steel blades, and the third to fifth stators were cast stainless-steel blades.

A photograph of the assembled compressor with the upper casing removed is shown in figure 8.

Lewis Flight Propulsion Laboratory
National Advisory Committee for Aeronautics
Cleveland, Ohio, June 18, 1954

[redacted]

3198

APPENDIX A

VELOCITY-DIAGRAM EQUATIONS

From reference 10, the basic radial equilibrium equation for steady axially symmetric ($\partial/\partial\theta = 0$) flow at an axial station between blade rows is given by the following (neglecting terms involving the coefficient of viscosity):

$$\frac{\partial H}{\partial r} = t\frac{\partial s}{\partial r} + \frac{V_\theta}{r}\frac{\partial(rV_\theta)}{\partial r} + V_x\frac{\partial V_x}{\partial r} - V_x\frac{\partial V_r}{\partial x} \tag{A1}$$

For the particular type of design used herein, the following design conditions were assumed:

(1) No radial variation of heat transfer or dissipation of energy by viscosity over the main portion of flow outside the wall boundary layers ($\partial s/\partial r = 0$). (This assumption loses some of its validity in the later stages as the flow area becomes smaller, but for simplicity it was used at all stations.)

(2) Negligible effect of streamline curvature in the r,x-plane ($\partial V_r/\partial x = 0$). According to reference 10, this assumption will be valid for a stage with low blade aspect ratio and large axial spacing between blade rows.

(3) Radially constant work input in all stages. Inasmuch as the total energy at the compressor inlet is constant radially and no work is done across the stators, a radially constant total energy will occur at all blade-row stations, that is, $\partial H/\partial r = 0$. The substitution of these three design conditions into the basic equation (A1) results in the simplified design equation

$$0 = \frac{V_\theta}{r}\frac{\partial(rV_\theta)}{\partial r} + V_x\frac{\partial V_x}{\partial r} \tag{A2}$$

At the rotor outlet, for constant rotor work input from hub to tip and no inlet rotation, a free-vortex rotation is required, given by

$$V_\theta = \frac{\text{constant}}{r} = \frac{r_t V_{\theta,t}}{r} \tag{A3}$$

and equation (A2) reduces to

$$V_x = \text{constant} \tag{A4}$$

Thus, the axial velocity will be constant radially at the rotor outlet.

For axial discharge at the stator outlet, $V_\theta = 0$, and from equation (A2)

$$V_x = \text{constant} \tag{A5}$$

The axial velocity is thus also radially constant at the outlet of each stator row.

At the rotor outlet (stator inlet), the tangential velocity at the tip (no inlet rotation) is related to the total-pressure ratio across the rotor according to

$$V_{\theta,t,n} = \frac{(a_T^2)_{n-1}}{(\gamma-1)\eta_{R,n} U_t}\left[\left(\frac{P_n}{P_{n-1}}\right)^{\frac{\gamma-1}{\gamma}} - 1\right] \tag{A6}$$

Total-pressure ratio is then related to total-temperature ratio through the adiabatic temperature-rise efficiency by the equation

$$\eta = \frac{\left(\frac{P_n}{P_{n-1}}\right)^{\frac{\gamma-1}{\gamma}} - 1}{\frac{T_n}{T_{n-1}} - 1} \tag{A7}$$

(Stage and over-all efficiencies were obtained from eq. (A7) by using stage and over-all total-temperature and total-pressure ratios.)

The continuity equation for the actual weight flow at rotor or stator outlet is

$$W = 2\pi K V_x \int_{r_h}^{r_t} \rho r \, dr \tag{A8}$$

and the density is given by

$$\rho = \frac{P}{RT}\left(1 - \frac{\gamma-1}{2}\frac{V^2}{\gamma g R T}\right)^{\frac{1}{\gamma-1}} \tag{A9}$$

The total velocity is related to its components, as shown in figure 4, by

$$V^2 = V_\theta^2 + V_x^2 + V_r^2$$

[redacted]

or

$$V^2 = V_\theta^2 + V_x^2 (1 + \tan^2 \varepsilon) \tag{A10}$$

The radial angle of the conic streamline surface ε is given by

$$\varepsilon = \tan^{-1} \frac{\Delta r}{\Delta x}$$

where Δr and Δx are the changes in radius and axial distance, respectively, of a streamline across the blade row from inlet to outlet (fig. 3).

3198

For compressor designs of high pressure ratio or short axial chord lengths, the value of the tangent plane angle ε may be relatively large (especially for an inlet stage), and the radial angle terms of the velocity-diagram equations cannot be neglected as was done in this design. Thus, for general use, complete equations are given below.

Velocity diagrams at the rotor inlet were computed from

$$V = \frac{V_x}{\cos \varepsilon} \tag{A11}$$

$$V' = \sqrt{U^2 + V_x^2 (1 + \tan^2 \varepsilon)} \tag{A12}$$

$$\beta^{*\prime} = \tan^{-1}\left(\frac{U}{V_x}\right) \cos \varepsilon \tag{A13}$$

Velocity diagrams at the rotor outlet (stator inlet) were computed from

$$V = \sqrt{V_\theta^2 + V_x^2 (1 + \tan^2 \varepsilon)} \tag{A14}$$

$$V' = \sqrt{(U - V_\theta)^2 + V_x^2 (1 + \tan^2 \varepsilon)} \tag{A15}$$

$$\beta^* = \tan^{-1}\left(\frac{V_\theta}{V_x}\right) \cos \varepsilon \tag{A16}$$

$$\beta^{*\prime} = \tan^{-1} \frac{(U - V_\theta)}{V_x} \cos \varepsilon \tag{A17}$$

Standard inlet total pressure and total temperature were taken, respectively, as 2116.8 pounds per square foot and 520° R.

3198
CT-3 back

APPENDIX B

EQUATION FOR HUB RADIUS RATIO

The actual weight flow passing through any axial station of the compressor may be expressed in terms of average flow conditions as

$$W = K\rho V_x \pi (r_t^2 - r_h^2) = K\rho V_x \pi r_t^2 (1 - z_h^2) \tag{B1}$$

where $z_h = r_h/r_t$, the hub radius ratio; ρV_x is an average value across a passage where free-stream conditions are considered to exist to the wall boundaries; and K is the boundary-layer blockage factor. From the energy equation, the static density is

$$\rho = \rho_T \left(1 - \frac{\gamma-1}{2} \frac{V^2}{g\gamma RT}\right)^{\frac{1}{\gamma-1}}$$

or, in terms of total pressure, total temperature, and axial velocity (neglecting radial velocities),

$$\rho = \frac{P}{RT} \left(1 - \frac{\gamma-1}{2} \frac{V_x^2}{g\gamma RT \cos^2\beta}\right)^{\frac{1}{\gamma-1}} \tag{B2}$$

The velocity of sound based on total temperature is given by

$$a_T^2 = g\gamma RT \tag{B3}$$

Combining equations (B2) and (B3) and substituting in equation (B1) then yield

$$W = KA_f \left(\frac{P}{RT}\right) V_x \left(1 - \frac{\gamma-1}{2} \frac{V_x^2}{a_T^2 \cos^2\beta}\right)^{\frac{1}{\gamma-1}} (1 - z_h^2) \tag{B4}$$

In terms of ratios based on compressor-inlet conditions,

$$W = KA_f \frac{P_0}{RT_0} \frac{\left(\frac{P}{P_0}\right)}{\left(\frac{T}{T_0}\right)} V_x \left[1.0 - \frac{\gamma-1}{2} \frac{V_x^2}{a_{T,0}^2 \left(\frac{T}{T_0}\right) \cos^2\beta}\right]^{\frac{1}{\gamma-1}} (1.0 - z_h^2) \tag{B5}$$

[redacted]

where P_0 and T_0 are total conditions at the compressor inlet. Solving for z_h then gives

$$z_h = \sqrt{1.0 - \frac{\left(\frac{W}{A_f K}\right)\left(\frac{RT_0}{P_0}\right)\frac{\sqrt{T/T_0}}{P/P_0}}{\frac{V_x}{\sqrt{T/T_0}}\left[1.0 - \frac{\gamma-1}{2}\frac{\left(\frac{V_x}{\sqrt{T/T_0}}\right)^2}{a^2_{T,0}\cos^2\beta}\right]^{\frac{1}{\gamma-1}}}} \qquad \text{(B6)}$$

For this design with axial-discharge stator blades, at each stage outlet $\beta = 0$ and the $\cos^2\beta$ term in equation (B6) was unity.

3198

REFERENCES

1. Lieblein, Seymour: Review of High-Performance Axial-Flow-Compressor Blade-Element Theory. NACA RM E53L22, 1954.

2. Lieblein, Seymour, Lewis, George W., Jr., and Sandercock, Donald M.: Experimental Investigation of an Axial-Flow Compressor Inlet Stage Operating at Transonic Relative Inlet Mach Numbers. I - Over-All Performance of Stage with Transonic Rotor and Subsonic Stators up to Rotor Relative Inlet Mach Number of 1.1. NACA RM E52A24, 1952.

3. Serovy, George K., Robbins, William H., and Glaser, Frederick W.: Experimental Investigation of a 0.4 Hub-Tip Diameter Ratio Axial-Flow Compressor Inlet Stage at Transonic Inlet Relative Mach Numbers. I - Rotor Design and Over-All Performance at Tip Speeds from 60 to 100 Percent of Design. NACA RM E53I11, 1953.

4. Geye, Richard P., Budinger, Ray E., and Voit, Charles H.: Investigation of a High-Pressure-Ratio Eight-Stage Axial-Flow Research Compressor with Two Transonic Inlet Stages. II - Preliminary Analysis of Over-All Performance. NACA RM E53J06, 1953.

5. Sandercock, Donald M., Lieblein, Seymour, and Schwenk, Francis C.: Experimental Investigation of an Axial-Flow Compressor Inlet Stage Operating at Transonic Relative Inlet Mach Numbers. IV - Stage and Blade-Row Performance of Stage with Axial-Discharge Stators. NACA RM E54C26, 1954.

6. Lieblein, Seymour, Schwenk, Francis C., and Broderick, Robert L.: Diffusion Factor for Estimating Losses and Limiting Blade Loadings in Axial-Flow-Compressor Blade Elements. NACA RM E53D01, 1953.

[redacted]

7. Kovach, Karl, and Sandercock, Donald M.: Experimental Investigation of a Five-Stage Axial-Flow Research Compressor with Transonic Rotors in All Stages. II - Over-All Performance. NACA RM E54G01, 1954.

8. Finger, Harold B., and Dugan, James F., Jr.: Analysis of Stage Matching and Off-Design Performance of Multistage Axial-Flow Compressors. NACA RM E52D07, 1952.

9. Hatch, James E., Giamati, Charles C., and Jackson, Robert J.: Application of Radial-Equilibrium Condition to Axial-Flow Turbomachine Design Including Consideration of Change of Entropy with Radius Downstream of Blade Row. NACA RM E54A20, 1954.

10. Wu, Chung-Hua, and Wolfenstein, Lincoln: Application of Radial-Equilibrium Condition to Axial-Flow Compressor and Turbine Design. NACA Rep. 955, 1950. (Supersedes NACA TN 1795.)

11. Klapproth, John F.: General Considerations of Mach Number Effects on Compressor-Blade Design. NACA RM E53L23a, 1954.

12. Erwin, John R., Savage, Melvyn, and Emery, James C.: Two-Dimensional Low-Speed Cascade Investigation of NACA Compressor Blade Sections Having a Systematic Variation of Mean-Line Loading. NACA RM L53I30b, 1953.

13. Andrews, S. J.: Tests Related to the Effect of Profile Shape and Camber Line on Compressor Cascade Performance. Rep. No. R.60, British N.G.T.E., Oct. 1949.

14. Robbins, William H., and Glaser, Frederick W.: Investigation of an Axial-Flow-Compressor Rotor with Circular-Arc Blades Operating up to a Rotor-Inlet Relative Mach Number of 1.22. NACA RM E53D24, 1953.

15. Herrig, L. Joseph, Emery, James C., and Erwin, John R.: Systematic Two-Dimensional Cascade Tests of NACA 65-Series Compressor Blades at Low Speeds. NACA RM L51G31, 1951.

3198

[redacted]

TABLE I. - STAGE CHARACTERISTICS USED IN FINAL DESIGN

Stage	Axial station	Stage efficiency, η	Stator-outlet axial velocity, V_x, ft/sec	Stage total-pressure ratio	Boundary-layer blockage factor, K
	2		648		0.99
1	4	0.890	620	1.390	.95
2	6	.885	600	1.480	.94
3	8	.875	570	1.425	.93
4	10	.870	550	1.350	.92
5	12	.850	520	1.265	.90

3198

[redacted]

TABLE II. - ROTOR VELOCITY-DIAGRAM DATA ON STREAMLINE (TANGENT) PLANE

Stage	Station	Entrance vectors						Change across row			Diffusion factor, D
		z	V_θ	V_x	V'	M'	β'	ΔV_θ	ΔV_x	Δβ', deg	
1	2	0.500	0	648	850	0.787	40.3	557	-53	33.9	0.4714
		.600	↓	↓	925	.857	45.5	483	↓	23.9	
		.700	↓	↓	1006	.932	49.9	427	↓	16.9	
		.800	↓	↓	1093	1.012	53.6	382	↓	12.1	
		.900	↓	↓	1183	1.096	56.8	346	↓	8.9	
		1.000	↓	↓	1277	1.183	59.5	316	↓	6.7	.3557
2	4a	0.620	0	651	943	0.826	46.3	634	-75	36.4	0.5646
		.696	↓	↓	1005	.880	49.6	577	↓	27.8	
		.772	↓	↓	1070	.937	52.5	529	↓	21.1	
		.848	↓	↓	1138	.997	55.1	488	↓	16.1	
		.924	↓	↓	1207	1.057	57.4	454	↓	12.5	
		1.000	↓	↓	1278	1.119	59.4	423	↓	9.8	.4456
3	6a	0.722	0	617	1005	0.821	52.2	583	-52	29.0	0.5503
		.778	↓	↓	1054	.861	54.2	546	↓	23.6	
		.833	↓	↓	1105	.903	56.1	514	↓	19.4	
		.889	↓	↓	1156	.944	57.8	485	↓	16.0	
		.944	↓	↓	1208	.987	59.3	460	↓	13.3	
		1.000	↓	↓	1261	1.030	60.7	437	↓	11.2	.4420
4	8a	0.778	0	595	1042	0.800	55.2	509	-54	21.0	0.5408
		.822	↓	↓	1083	.832	56.7	485	↓	17.8	
		.867	↓	↓	1123	.863	58.0	462	↓	15.0	
		.911	↓	↓	1165	.895	59.3	442	↓	12.9	
		.956	↓	↓	1208	.928	60.5	423	↓	11.1	
		1.000	↓	↓	1251	.961	61.6	406	↓	9.5	.4393
5	10a	0.816	0	572	1065	0.777	57.5	445	-48	16.2	0.5163
		.853	↓	↓	1099	.801	58.6	426	↓	13.9	
		.890	↓	↓	1134	.827	59.7	408	↓	12.0	
		.926	↓	↓	1169	.852	60.7	391	↓	10.4	
		.963	↓	↓	1204	.878	61.7	376	↓	9.1	
		1.000	↓	↓	1240	.904	62.5	362	↓	7.9	.4175

TABLE III. - STATOR VELOCITY-DIAGRAM DATA ON STREAMLINE (TANGENT) PLANE

Stage	Station	Entrance vectors						Change across row			Diffusion factor, D
		z	V_θ	V_x	V	M	β	ΔV_θ	ΔV_x	$\Delta\beta$, deg	
1	3	0.570	557	595	815	0.730	43.1	557	25	43.1	0.4321
		.656	483	↓	766		39.1	483	↓	39.1	
		.742	427		732		35.7	427		35.7	
		.828	382		707		32.7	382		32.7	
		.914	346		688		30.2	346		30.2	
		1.000	316		674	.592	28.0	316		28.0	.3023
2	5	0.675	634	576	857	0.717	47.8	634	24	47.8	0.5009
		.740	577	↓	815		45.1	577	↓	45.1	
		.805	529		782		42.6	529		42.6	
		.870	488		755		40.3	488		40.3	
		.935	454		733		38.2	454		38.2	
		1.000	423		715	.589	36.3	423		36.3	.3933
3	7	0.753	583	565	812	0.635	45.9	583	5	45.9	0.5226
		.802	546	↓	786		44.0	546	↓	44.0	
		.852	514		764		42.3	514		42.3	
		.901	485		745		40.6	485		40.6	
		.951	460		729		39.2	460		39.2	
		1.000	437		714	.554	37.7	437		37.7	.4559
4	9	0.799	509	541	743	0.548	43.2	509	9	43.2	0.4938
		.839	485	↓	727		41.9	485	↓	41.9	
		.879	462		711		40.5	462		40.5	
		.920	442		699		39.2	442		39.2	
		.960	423		687		38.0	423		38.0	
		1.000	406		676	.496	36.9	406		36.9	.4431
5	11	0.825	445	524	687	0.484	40.3	445	-4	40.3	0.4786
		.860	426	↓	675		39.1	426	↓	39.1	
		.895	408		664		37.9	408		37.9	
		.930	391		654		36.7	391		36.7	
		.965	376		645		35.7	376		35.7	
		1.000	362		637	.447	34.6	362		34.6	.4343

[redacted]

TABLE IV. - ROTOR BLADE DESIGN DATA ON HORIZONTAL PLANE

[Leading- and trailing-edge radii, 0.015 in.]

Stage	Number of blades	Radius ratio, x	Hub axial chord length, $c_{h,x}$, in.	Actual chord length, c, in.	Solidity, σ	Incidence angle, i, deg	Deviation angle, δ^*, deg	Camber angle, φ, deg	Setting angle, ξ, deg	Maximum thickness, percent chord	Suction-surface radius, in.	Pressure-surface radius, in.	Mean-line radius, in.
1	23	0.500	2.50	2.58	1.89	4	9	58.4	8.9	8	2.18	3.46	2.64
		.600		2.61	1.59	↓	↓	40.3	22.4		2.92	5.64	3.80
		.800		2.67	1.22			19.9	40.2		5.06	16.83	7.72
		1.000		2.68	.98			11.7	49.7	5	7.51	55.41	13.11
2	27	0.620	2.50	2.68	1.86	4	9	52.1	17.4	8	2.45	4.23	3.06
		.696		2.69	1.66	↓	↓	40.0	26.3		3.01	5.85	3.92
		.848		2.72	1.38			23.7	39.6		4.60	12.15	6.63
		1.000		2.73	1.17			14.8	48.0	5	6.64	26.02	10.57
3	28	0.722	2.50	2.86	1.77	4	10.2	42.4	27.9	8	2.98	6.15	3.95
		.778		2.87	1.64	↓	9.5	34.1	33.7		3.56	8.12	4.89
		.889		2.88	1.44		8.1	21.7	43.2		5.15	15.59	7.66
		1.000		2.93	1.30		6.7	13.8	49.8	5	7.42	36.21	12.20
4	25	0.778	2.25	2.86	1.46	4	9.9	26.8	37.8	8	3.96	14.96	6.16
		.822		↓	1.38	↓	9.4	23.1	41.1		4.53	17.74	7.12
		.911			1.25		8.5	17.3	46.7		5.87	26.60	9.50
		1.000			1.14		7.5	13.0	51.1	5	7.51	41.68	12.65
5	23	0.816	2.00	2.71	1.21	4	10.3	22.4	42.3	8	4.17	23.13	6.96
		.853		↓	1.16	↓	9.9	19.7	44.8		4.73	28.43	7.91
		.926			1.07		9.0	15.4	49.0		5.96	34.55	10.12
		1.000			.99		8.2	12.0	52.5	5	7.48	50.15	12.90

TABLE V. - STATOR BLADE DESIGN DATA ON HORIZONTAL PLANE

[Leading-edge radius, 0.015 in. for stages 1 and 2, 0.023 in. for stages 3, 4, and 5; trailing-edge radius, 0.015 in. for all stages.]

Stage	Number of blades	Radius ratio, z	Tip axial chord length, $c_{t,x}$, in.	Actual chord length, c, in.	Solidity, σ	Incidence angle, i, deg	Deviation angle, δ^*, deg	Camber angle, φ, deg	Setting angle, ξ, deg	Maximum thickness, percent chord	Suction-surface radius, in.	Pressure-surface radius, in.	Mean-line radius, in.
1	33	0.570		2.025	1.80	0	2.3	45.6	19.8	6.5	2.15	3.41	2.61
		.656		↓	1.62	↓	4.3	43.8	16.8		2.20	3.66	2.72
		.828			1.28		9.6	42.4	11.2		2.20	3.98	2.80
		1.000	2.00		1.06		17.0	45.0	5.5	8	2.06	3.84	2.65
2	39	0.675		2.050	1.89	0	3.0	50.4	22.2	6.5	2.03	3.03	2.41
		.740		↓	1.72	↓	5.0	50.1	19.7		2.02	3.10	2.42
		.870			1.46		7.2	47.7	16.2		2.05	3.42	2.54
		1.000	2.00		1.27		11.0	47.3	12.7	8	2.02	3.62	2.56
3	37	0.753		2.044	1.60	-2	6.5	54.4	20.7	9			2.24
		.877		↓	1.37	↓	11.0	54.5	16.2				2.23
		1.000	2.00		1.20		16.0	55.7	11.9	10			2.19
4	36	0.799		2.042	1.46	-2	7.5	52.7	18.9	9			2.30
		.900		↓	1.30	↓	11.3	53.1	15.3				2.29
		1.000	2.00		1.17		15.5	54.4	11.7	10			2.23
5	35	0.825		2.036	1.38	-2	8.0	50.3	17.2	9			2.40
		.913		↓	1.24	↓	11.5	50.8	13.9				2.37
		1.000	2.00		1.13		15.0	51.6	10.8	10			2.34

3198 CT-4 back

TABLE VI. - THICKNESS DISTRIBUTION FOR A 10-PERCENT-MAXIMUM-THICKNESS 65-SERIES BLADE[1]

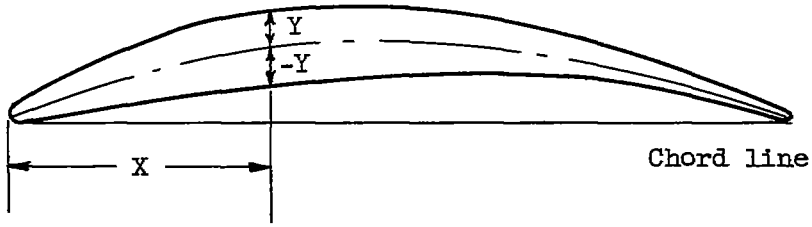

X, percent chord	±Y, percent chord	X, percent chord	±Y, percent chord
0	0	55	4.530
.5	.772	60	4.146
.75	.932	65	3.611
1.25	1.169	70	3.123
2.5	1.574	75	2.643
5.0	2.177	80	2.188
7.5	2.647	85	1.762
10	3.040	90	1.369
15	3.666	95	1.037
20	4.143	100	.800
25	4.503		
30	4.760		
35	4.924		
40	4.996		
45	4.963		
50	4.812		

[1]Other thicknesses scale proportionately.

[redacted]

3198

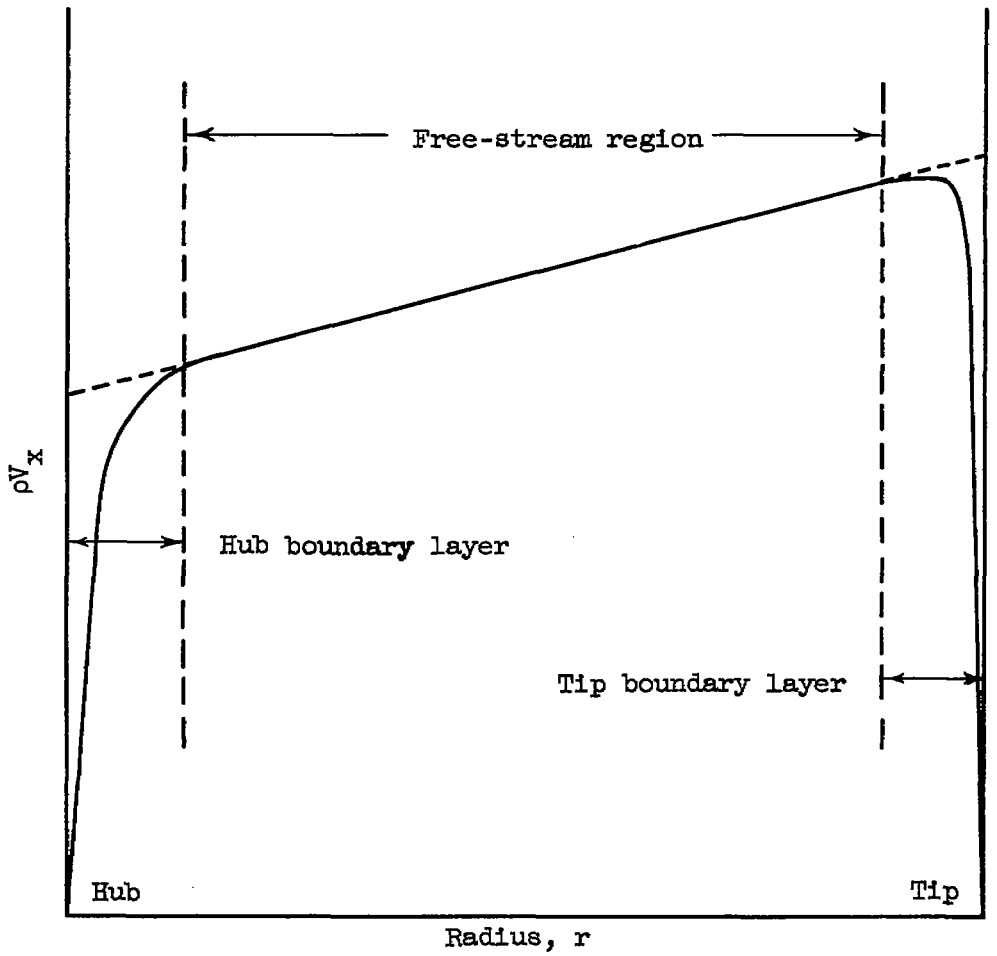

Figure 1. - Assumed radial division of flow at blade-row outlet illustrating free-stream and boundary-layer regions.

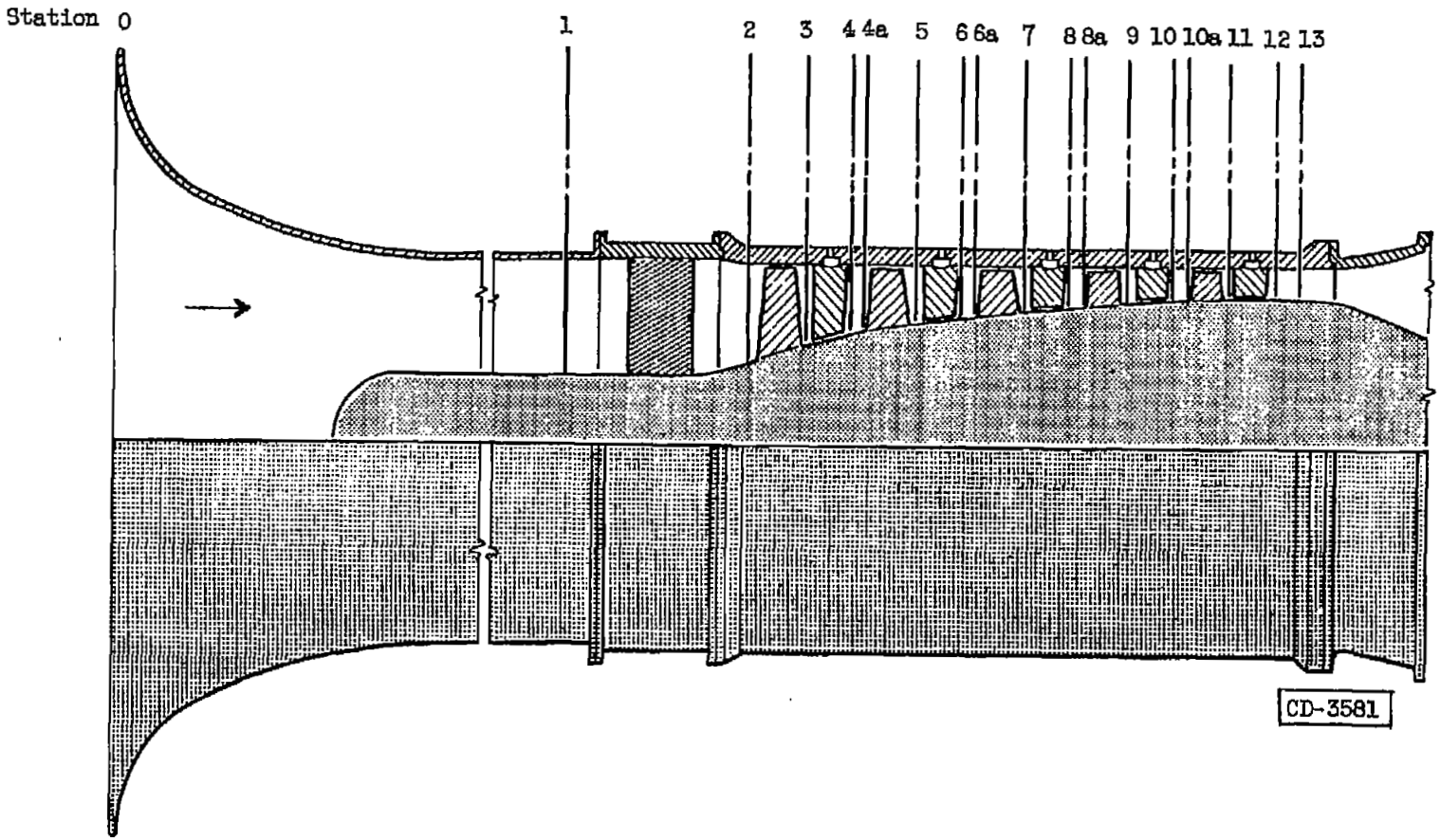

Figure 2. - Sketch of passage contour of five-stage axial-flow transonic compressor showing axial location of blade-row-inlet and -outlet stations.

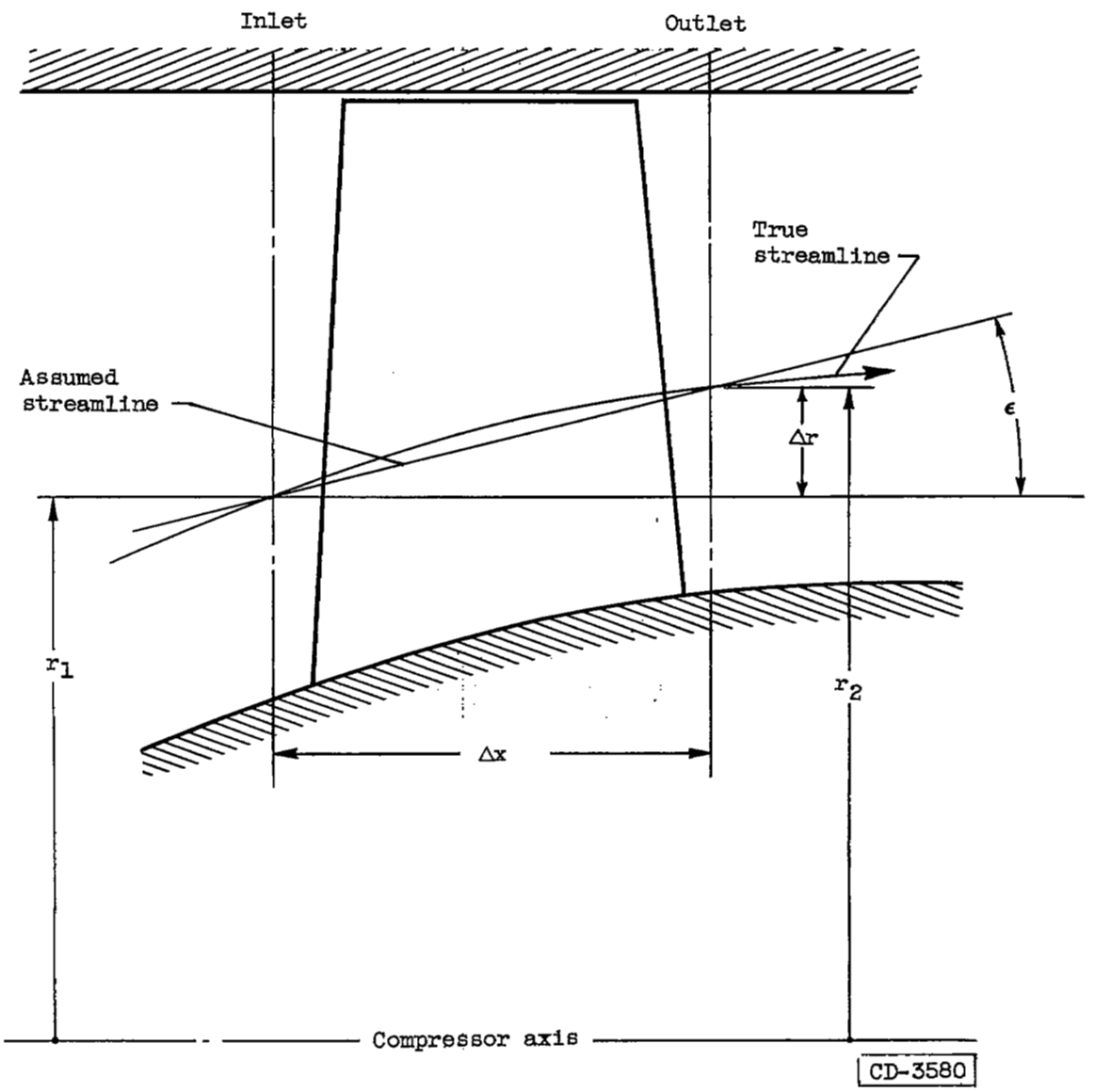

Figure 3. - Sketch illustrating radial angle of assumed conic streamline surface.

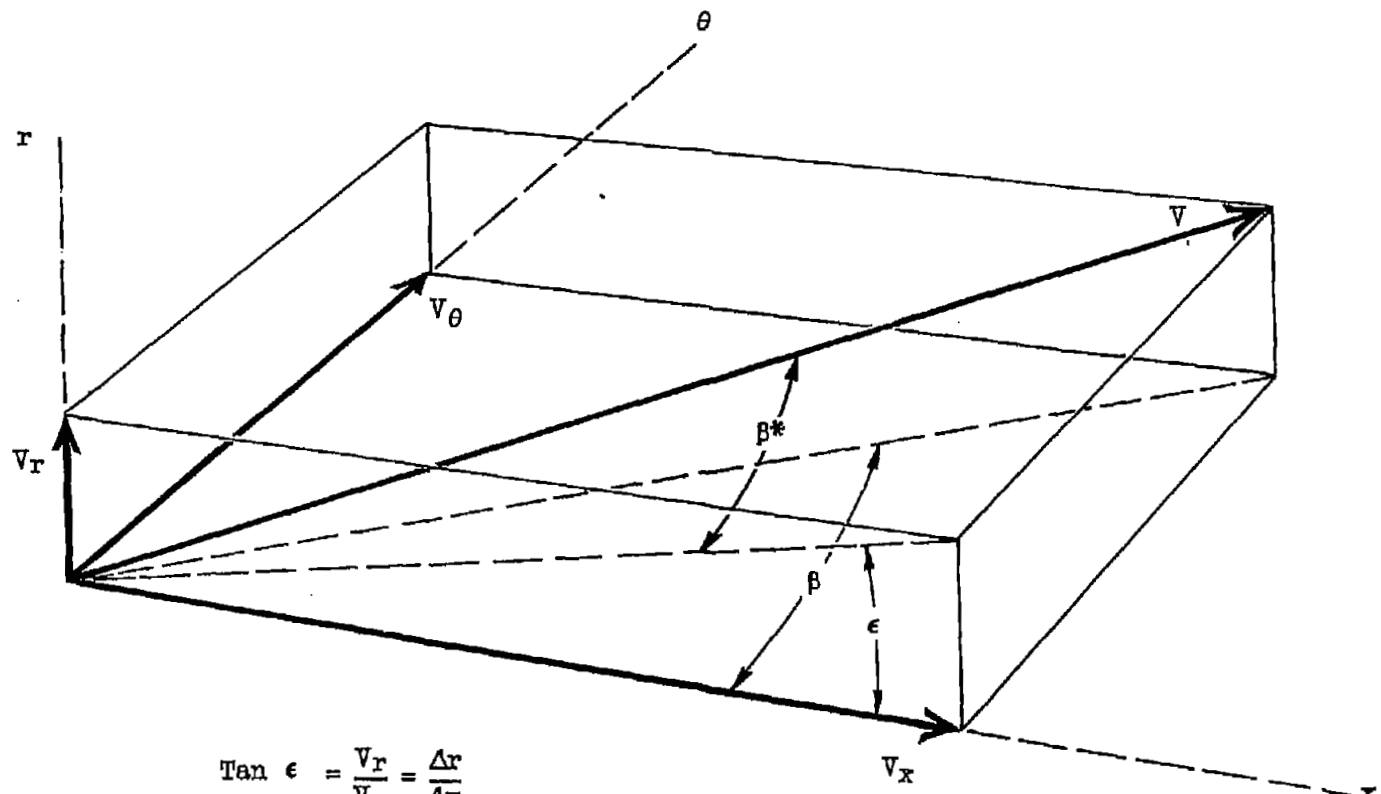

$$\text{Tan } \epsilon = \frac{V_r}{V_x} = \frac{\Delta r}{\Delta x}$$

$$\text{Tan } \beta^* = \tan \beta \cos \epsilon$$

$$= \frac{V_\theta}{V_x} \cos \epsilon$$

Figure 4. - Relationships between total velocity and its components.

3198

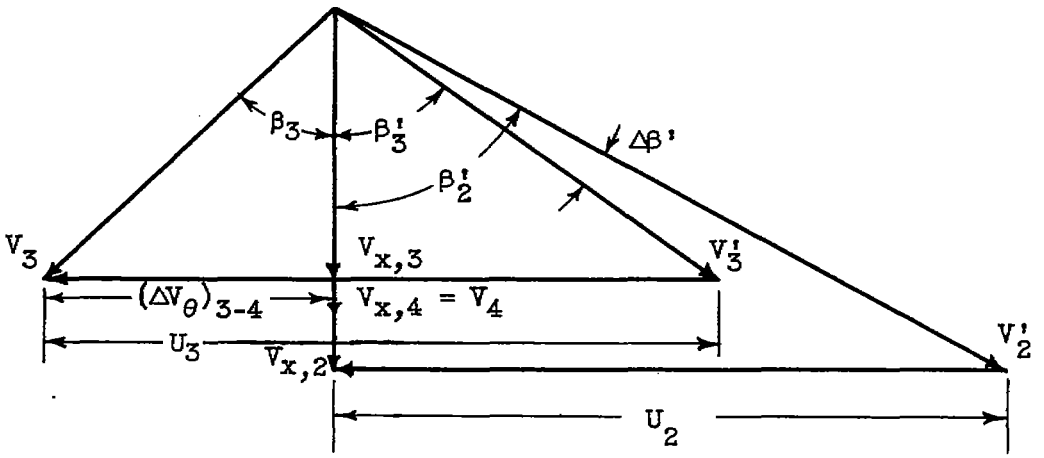

(a) Tip.

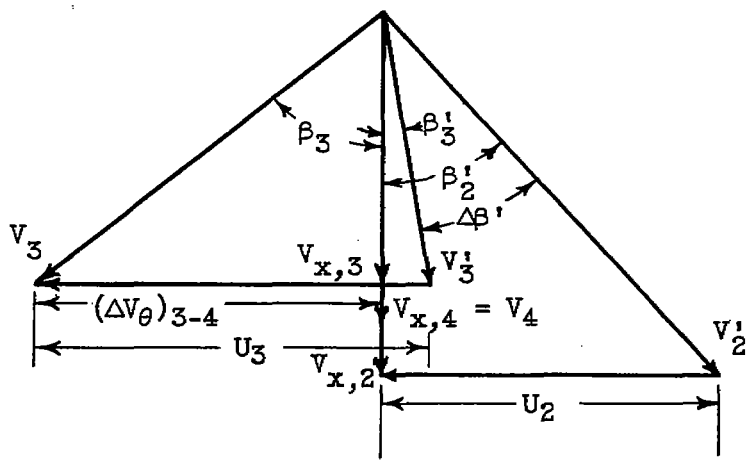

(b) Hub.

Figure 5. - Schematic sketch of velocity diagrams for first-stage rotor and stator at hub and tip radii. [Stator diagram represented by absolute (left side) portion of diagram.]

3198

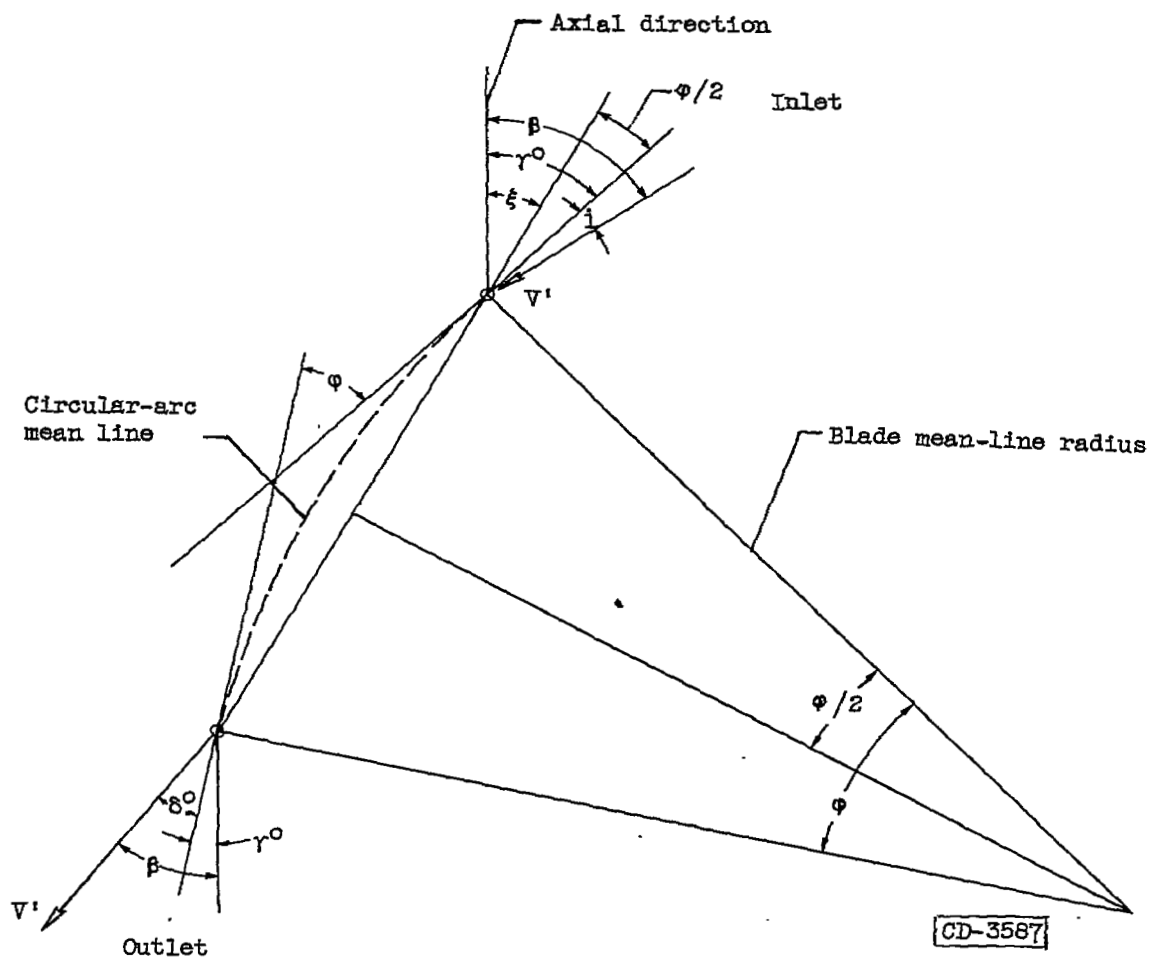

$$\Delta\beta' = \beta'_{inlet} - \beta'_{outlet}$$

$$\varphi = \gamma^{\circ}_{inlet} - \gamma^{\circ}_{outlet}$$

$$\xi = \frac{\gamma^{\circ}_{inlet} + \gamma^{\circ}_{outlet}}{2}$$

Figure 6. - Sketch of angles used to compute blade properties.

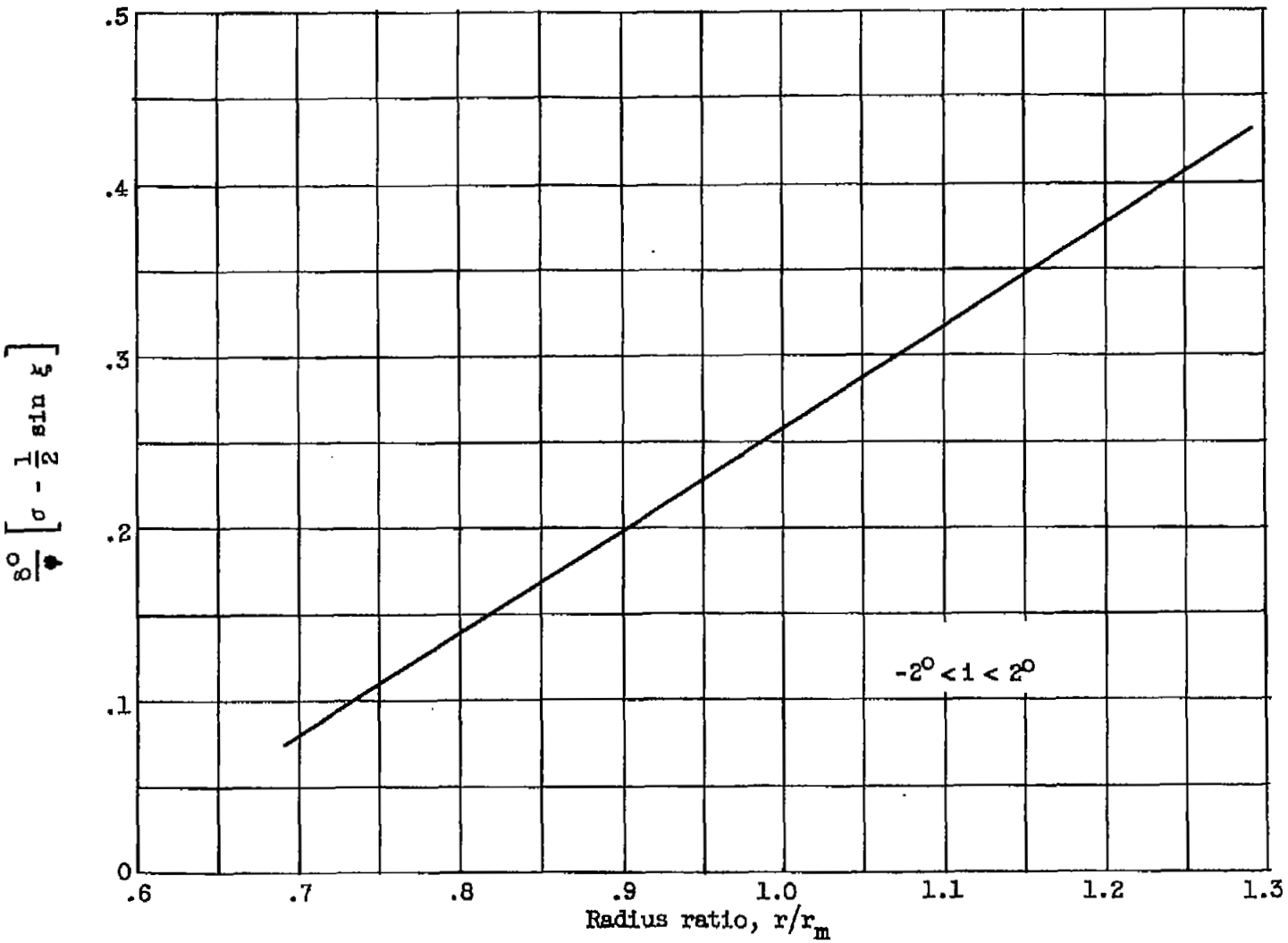

Figure 7. - Design values of deviation-angle parameter for stator blades.

NACA-Langley - 8-8-54 - 350

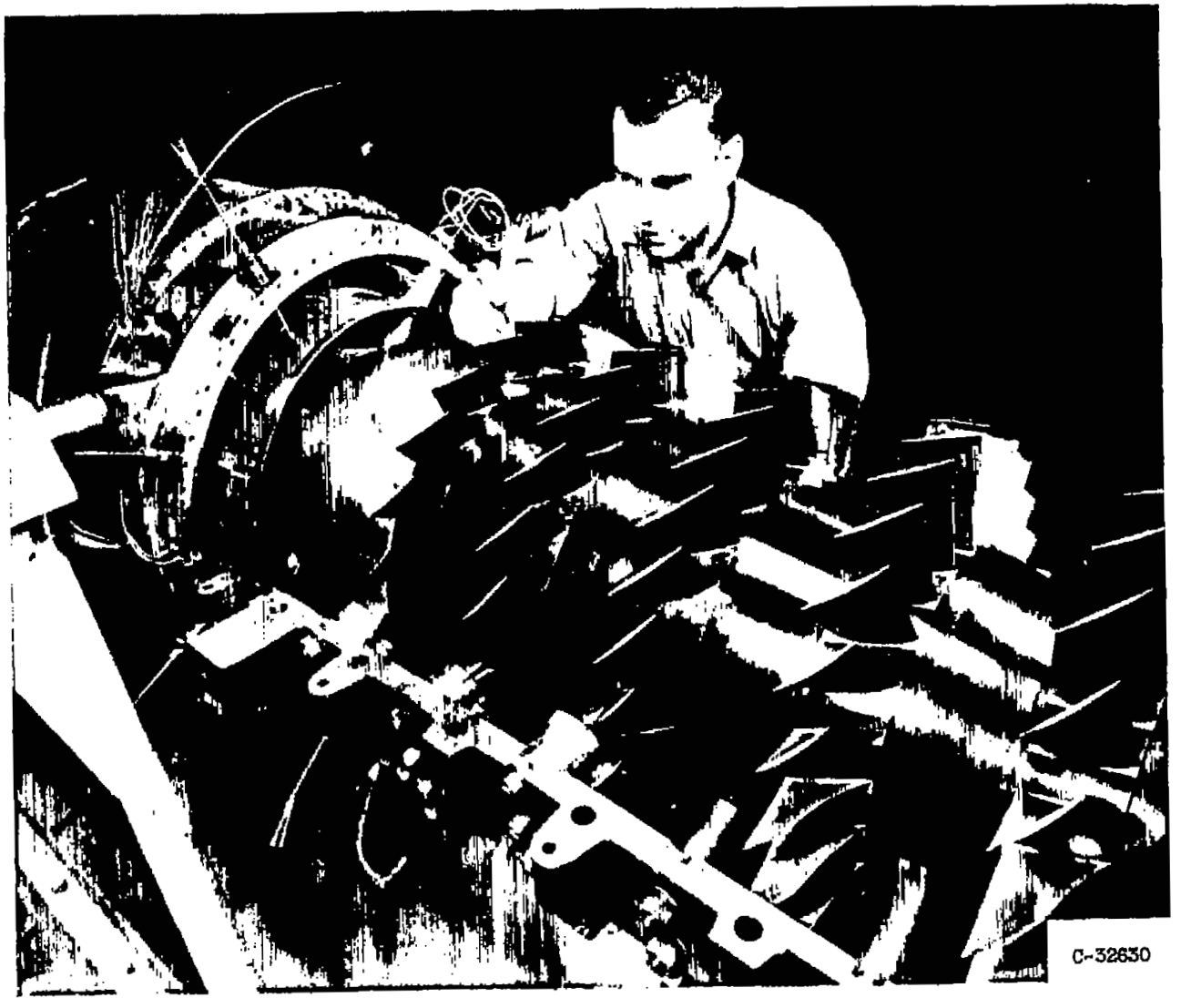

Figure 8. - Photograph of five-stage axial-flow transonic compressor with upper casing removed.